JOURNAL OF PROPULSION AND POWER
Vol. 22, No. 5, September–October 2006

Simulation of Void Collapse in an Energetic Material, Part 1: Inert Case

L. Tran*
Naval Postgraduate School, Monterey, California 93943
and
H. S. Udaykumar†
University of Iowa, Iowa City, Iowa 52242

An Eulerian, sharp-interface, fixed Cartesian grid method is applied to study hot-spot formation in an energetic material (HMX) subject to shock loading. The mass, momentum, and energy equations are solved along with evolution equations for deviatoric stresses and equivalent plastic strain. Pressure is obtained from the Mie–Grüneisen equation of state. The material is modeled as a viscoplastic solid. High-order accurate essentially-nonoscillatory (ENO) shock-capturing schemes along with a particle-level set technique are used to evolve sharp immersed boundaries. The details of void collapse under shock loading and the resulting conversion of mechanical energy into localized regions of high thermal energy (hot spots) in the solid material are analyzed. Insights into the precise mechanisms of initiation sensitivity as a result of hot-spot formation in porous energetic materials are obtained.

I. Introduction

INITIATION of an energetic material or high explosive can occur when an impulse delivered to the material evolves into a self-sustaining detonation wave. Wave growth towards detonation depends on the formation of local regions of elevated thermal energy or hot spots, where local temperatures can be much higher than the bulk temperature expected from shock heating. When sufficient thermal energy is generated locally, ignition occurs, and subsequent chemical energy release results in progressive shock strengthening until detonation conditions are achieved. This concept was first proposed by Bowden and Yoffe.[1] One site where such energy focusing (hot spots) can occur is at a void in the material.

Porosities or voids in heterogeneous explosives offer potential sites for the initiation of detonations. Khasainov et al.[2] have characterized the different regimes of initiation of detonation through the void-collapse mechanism. Assuming that in a solid high explosive (HE), voids collapse when the shock strength exceeds the yield strength of the material

$$P_s > (2Y/3)\,\ell n(1/\phi) = P_Y \tag{1}$$

where P_s, P_Y, Y, and ϕ are the shock strength, critical shock strength, yield strength of the material, and porosity of the material. A typical value for the critical shock strength P_Y in an HE is 0.1–0.3 GPa. The mode of collapse depends on several parameters, such as the initial pore size, material viscosity, and the shock pressure. Khasainov et al. define a critical pore size:

$$\delta_c = 8.4\mu_s \Big/ \sqrt{\rho_s(P_s - P_Y)} \tag{2}$$

where δ_c, μ_s, ρ_s are the critical pore size for viscous flow, solid-phase viscosity, and solid-phase density, respectively. Based on the initial pore size δ_0 of a particular pore, a Reynolds number is defined for the void such that

$$Re = \delta_0/\delta_c = 2\delta_0\sqrt{\rho P_s}\Big/\mu_s \tag{3}$$

For small Reynolds numbers the void collapse can be considered to be in the viscous regime, whereas for large Reynolds numbers the collapse is in the hydrodynamic regime. Instead of a length scale one can also view the preceding characterization in terms of timescales so that the characteristic time of collapse of a void is

$$t_\mu = 4\mu_s/(P_s - P_Y) \tag{4}$$

whereas the characteristic passage time for a shock is

$$t_p = \delta_0/U_s \tag{5}$$

where U_s is the shock velocity.

By the preceding criterion if the shock passage time is short compared to the void collapse time, the void-collapse mechanism can be considered to be in the viscous regime.

A number of mechanisms for the formation of hot spots at cavities have been proposed over the years. The applicability of these mechanisms depends on the strength of the imposed shock that initiates the explosion, and the regimes of operation can be identified roughly by the preceding criterion. Also, several mechanisms can play a role in a given hot-spot formation regime, depending on the pore size, shock strength, reactive characteristics of the material, etc. The mechanisms in approximate order of importance to HE initiation can be listed as follows:

1) *Viscoplastic:* When a solid material undergoes viscoplastic deformation, the temperature rise is caused by the conversion of viscoplastic work into heat. Significant heating can occur as a result of cavity collapse in very small cavities of less than 1 μm and in very short times of less than a microsecond.[2] Thus, this regime dominates in the lower-Reynolds-number regimes of void collapse as characterized by Eq. (3). The viscoplastic work in deforming the void is transformed to heat in a layer at the surface of the void. The extent of this layer is critical to the initiation mechanism. If the layer is too thin and the thermal energy is conducted away too rapidly from this layer before ignition of the reactive solid material can result, the explosion cannot be sustained. If the layer is too thick and the energy deposited is too diffuse, the temperature rise is not sufficient to cause initiation. Thus, smaller pores might not be effective sites of initiation because the heated layer surrounding them is very thin. In fact, the lower the shock pressure, the larger must be the pores that are responsible for ignition.

2) *Hydrodynamic:* When a high-explosive material is shock-loaded, as the shock wave propagates through a porous solid, the deformation occurs sequentially in the following modes: elastic, elastoplastic, and totally plastic. If the wave amplitude far exceeds

Received 31 August 2004; revision received 18 November 2005; accepted for publication 18 November 2005.

*Postdoctoral Research Associate, Department of Physics.
†Associate Professor, Department of Mechanical and Industrial Engineering.

the yield strength, the lower surface (i.e., the one facing the impinging shock) of the void deforms, forming a high-speed jet of material that impacts against the upper surface. This jet or hydrodynamic impact produces high impact pressures and temperatures as a result of the conversion of kinetic energy to heat, and this pressure buildup is amplified by convergence effects during cavity collapse.[3] In this mechanism, heating is produced by compression of the solid-phase material. This mechanism therefore corresponds to the high-Reynolds-number regime according to the definition in Eq. (3).

3) *Compression of gas in cavities:* As the voids collapse, the entrapped gas within them is compressed to high temperature and pressure. The temperature can reach a value high enough to initiate ignition. This mechanism can be dominant under conditions when the compression rate is relatively low and the voids are of the order of a millimeter or larger.[4,5] An alternate role is attributed to the gaseous-phase reaction in the viscous regime of collapse. The reaction starts in the gas phase as the viscous dissipation of the plastic work during deformation causes the heating of the material. After the reaction has been initiated in the vicinity of the pores, it propagates as a surface burning wave into the solid. The surface burning deposits gaseous reaction products into the void, which increases the gaseous pressure. Under suitable conditions, this gaseous pressure will eventually exceed the solid-phase pressure and cause a reversal of the plastic flow around the pore. This accelerates the surface burning and generates a secondary compression wave. This compression wave then interacts with the primary shock wave to enhance it.

Shear banding: When a high-explosive material is shocked, shear bands could form in the vicinity of collapsing cavities. Analysis[6] indicated that both pressure and shear rate are important parameters controlling the temperature. A shear banding mechanism for hot-spot formation could provide the large ignited surface area that is believed to be necessary to explain shock initiation.

Thus, the formation of hot spots at voids in a HE can involve several mechanisms, depending on the regime determined by the pore size, shock strength, and material characteristics. In all cases, the possibility of initiation hinges on the balance (or lack thereof) between thermal energy-producing mechanisms (viscoplastic work, kinetic energy, chemical reaction, gaseous compression, viscous shear) and the rate at which the energy is transported away by heat conduction without establishment of a feedback to detonation.

II. Models of Hot-Spot Formation

Most of the theories for impact ignition require the formation of hot spots, as the impact energy has generally been considered to be insufficient to heat the bulk material to the ignition temperature. It is also well known that porosity is an important parameter determining the sensitivity of explosives to shock waves and that cavities in an explosive act as sites where hot spots can occur. The burn rates of heterogeneous HEs subject to external loading such as impact/shocks display enhanced sensitivity to pressure when compared to laminar deflagration in such materials. Whereas in the latter case linear dependency on pressure is the norm, for heterogeneous explosives en route to detonation induced by external loading, quadratic pressure dependency is observed.[7] Such enhanced pressure dependency reflects the initiation of the combustion process at voids present in the porous explosive, which, upon collapse under applied compressive loads, lead to localized hot spots in the material.[8] The dependency on pressure is particularly relevant in shock- or impact-induced detonation of porous HE. Thus, models that analyze and predict the behavior of HE at the large-scale employ pressure-dependent, typically empirical, reaction-rate expressions. To move from empiricism to true understanding and predictive capabilities, in recent years, microscale (dynamics of a single void such as by Frey[7]) and mesoscale (dynamics of a material with distributed porosity such as by Menikoff and Kober[9]) models of detonation initiation of HE have been developed. Powers[10] has modeled the granular material using a continuum mixture theory to capture the heterogeneities in the explosive, with the microscale mechanisms modeled using subgrid models. The interactions that occur at the microscale are included in the mixture formulation as interphase exchange terms for mass, momentum, and energy exchange. Gonthier[11] has taken a more micromechanical approach and analyzed the contact mechanics of ordered spherical grains in order to analyze the effect of localized inelastic deformation and intergranular friction on the formation of hot spots. These works have attempted to characterize the meso- and macroscale signatures of localized events arising from the dynamics of microscale heterogeneities embedded in a typical granular HE. Recently, Gonthier and Jogi[12] have employed their micromodel in a multiscale analysis of shock heating of a granular explosive. The grain scale response is embedded within a bulk scale system of equations as a subgrid model.

Analyses of the response of individual voids to external loading have been performed in various limited settings by many researchers. Using a hollow sphere model, Khasainov et al.[2] discussed the formation of hot spots by the ductile collapse of spherical cavities, assuming an instantaneous rise in pressure and ignoring melting. In their work, the heating was exclusively a result of viscoplastic work. They found that significant heating can occur for very small cavities and in very short times. In a similar problem, but with a rate-independent stress, Carroll and Holt[13] found that very high temperatures can be produced by plastic work in the vicinity of collapsing cavities, but cavity size had no effect on the temperature. Using the same hollow sphere configuration, Kang et al.[5] included thermal processes such as finite-rate chemical effects, and heat exchange between the pore gas and the surrounding material. Two gas-phase chemical reaction mechanisms were examined, that is, a single-step reaction and multiple-step reactions, along with variable yield strength and viscosity. Viscoplastic heating was found to be an effective mechanism for shock initiation of porous, energetic materials.

Using a hollow cylinder, shear banding was considered by Powers[14] to predict ignition. The model considered was transient, one-dimensional, and included effects of thermal diffusion, plastic work, exothermic reaction with one-step irreversible Arrhenius kinetics, and a power-law constitutive model for shear stress. The model predicted reactive shear localization after an induction time of approximately 5 μs.

The constituent properties of HMX were discussed by Menikoff and Sewell.[15] They analyzed available experimental and theoretical physical parameters of HMX. These properties are needed for computations with mesoscale models. At grain level, an explosive is crystalline and, by its very nature, anisotropic. They found that this has an effect on the dissipative mechanisms leading to the formation and evolution of hot spots. Three-dimensional mesoscale models have often involved an idealized material structure. Typically, HMX crystals are modeled as regularly stacked spheres. A method for importing the actual microstructure of HMX material directly into a finite element calculation was developed by Benson and Conley.[16] In these mesoscale simulations, it was found that viscosity spreads out the shock front, reduces the temperature extremes, and suppresses particle-scale jetting. In a three-dimensional, idealized mesoscale calculation using the CTH code,[17] Baer et al.[18] simulated the processes of consolidation, deformation, and reaction of shocked porous explosive consisting of discrete HMX crystals. They showed that rapid deformation occurs at material contact points and localization of energy produces hot spots as a result of shock focusing and plastic work near grain boundaries. They found that hot spots are strongly influenced by multiple HMX crystal interactions and that the initiation and reaction of shocked heterogeneous materials involve states distinctly different from single jump state descriptions. In the HMX propellant, localized melting occurs, and two very distinct phases, a solid layer and a rubbery-viscous ("melt") layer, are formed during high strain-rate impact. Ignition occurs in the rubbery-viscous phase.

Modeling of the microscale rather than the mesoscale response of a heterogeneous explosive in the presence of voids remains a challenging task. The collapse of a void under the effects of an imposed shock loading involves several complex physical phenomena, including nonlinear stress wave propagation, evolution of a free surface of the void, topological changes as the void collapses

and disappears, and change of phase and reactive mechanics in the solid and gas phases. In this paper, a numerical method developed in Udaykumar et al.[19] and Tran and Udaykumar[20] is applied to study the microscale response of a void in a shocked energetic material. The numerical method has been thoroughly validated, and the void surface is tracked as a sharp entity in the method. Appropriate jump conditions are applied at the surface of the void. This paper examines the energetics of void collapse in the absence of chemical reactions. The objectives of the paper are as follows:

1) The first is to solve the difficult moving boundary problem of void collapse under shock loading using an Eulerian, sharp-interface technique.

2) The second is to include the leading-order mechanisms, that is, inertia and elastoplastic deformation to understand their interaction in void collapse and thermal energy localization. The focus therefore is on the mechanism of energy deposition and the contribution of viscoplastic work and kinetic energy to thermal energy localization. For this reason, thermal diffusion is not included in the energy equation as a transport mechanism for heat. Furthermore, for the pore sizes considered and the shock conditions applied the pore collapse times are in the range of nanoseconds. Although not shown explicitly in this paper, inclusion of thermal diffusion had a negligible effect on the thermal transport over the short period of void collapse encountered in the cases presented herein.

3) The final objective is to examine the effects of void size and shape in the extent of energy localization.

In keeping with the preceding objectives, physical mechanisms that are either incompletely characterized or that play secondary roles in the collapse and energy deposition process are not included in the model. Therefore, the present model provides focused treatment of interplay between inertia and plastic work in the void collapse problem. A more complete and "predictive" model of void collapse will need to include effects such as variation of thermal and mechanical properties of the material under pressure and temperature, effects of phase change in the material, both in the bulk as well as the free surface of the void, and unresolved physics, such as shear band formation, material fracture, and grain-boundary effects. Clearly, the complications entailed by these mechanisms delay the feasibility of a "predictive" model. As an extension of the inert model presented in this paper, part 2 in Tran and Udaykumar's[21] paper includes chemical heat release in the solid and gas phases and gas–solid interaction effects in the simulation of void collapse.

III. Formulation of the Problem

A. Constitutive Relations

The equations governing the material deformation appropriate for high-strain-rate applications can be formulated by assuming that the volumetric or dilatational response is governed by an equation of state while the shear or deviatoric response obeys a conventional flow theory of plasticity. The system of equations describing the material deformation in Lagrangian form can be written as follows. The stress in the material is expressed as the sum of the dilatational and deviatoric parts:

$$\sigma_{ij} = s_{ij} - p\delta_{ij} \tag{6}$$

Here σ_{ij} is the Cauchy stress tensor, s_{ij} its deviatoric part, and the hydrostatic pressure p taken to be positive in compression.

The rate of change of deviatoric stress is given by

$$s'_{ij} = 2G\left(\bar{D}_{ij} - D^p_{ij}\right) \tag{7}$$

$$s'_{ij} = \frac{\mathrm{d}s_{ij}}{\mathrm{d}t} + s_{ik}\Omega_{kj} - \Omega_{ik}s_{kj} \tag{8}$$

where G is the shear modulus, s'_{ij} the Jaumann derivative of s_{ij}, $\bar{D}_{ij}$ the deviatoric strain rate, D^p_{ij} the plastic strain rate, and Ω_{ij} the spin tensor. The Jaumann derivative is used to ensure material frame indifference with respect to rotation.

The spin tensor and the strain-rate tensor are given by

$$\Omega_{ij} = \tfrac{1}{2}(v_{i,j} - v_{j,i}) \tag{9}$$

$$D_{ij} = \tfrac{1}{2}(v_{i,j} + v_{j,i}) \tag{10}$$

where $D_{ij} = D^e_{ij} + D^p_{ij}$ is the strain-rate tensor composed of the elastic strain rate D^e_{ij} and the plastic strain rate D^p_{ij} and v_i is a velocity component. The notation $v_{i,j}$ denotes the spatial derivative of the velocity field.

The deviatoric strain rate is

$$\bar{D}_{ij} = D_{ij} - \tfrac{1}{3}D_{kk}\delta_{ij} \tag{11}$$

The plastic strain rate follows the relationships:

$$tr\left(D^p_{ij}\right) = 0 \tag{12}$$

$$D^p_{ij} = \Lambda N_{ij} \tag{13}$$

where $N_{ij} = s_{ij}/\sqrt{(s_{kl}s_{kl})}$ is the unit outward normal to the yield surface and Λ a positive consistency parameter.

The effective stress and effective plastic strain rate are given by

$$S^2_e \equiv \frac{3}{2}tr(s_{ij}s_{ji}) \tag{14}$$

$$\left(\frac{\mathrm{d}}{\mathrm{d}t}\bar{\varepsilon}^p\right)^2 = \frac{2}{3}tr\left(D^p_{ij}D^p_{ij}\right) \tag{15}$$

The overall pressure in a solid can be expressed as a sum of two terms, the pressure caused by the thermal excitation of atoms/molecules and the pressure resulting from the attractive/repulsive forces between them. For the present work, because of the high strain-rate, large deformation problem of concern, we utilize the Mie–Grüneisen on equation of state (e.o.s). If e_c and p_c denote respectively the "cold" (at 0 K) energy and pressure, the incomplete, temperature-independent formulation of the Mie–Grüneisen e.o.s. is

$$p(e, V) \sim \Gamma(V)\{[e - e_c(V)]/V\} + p_c(V) = \Gamma(e/V) + f(V) \tag{16}$$

where, by definition,

$$e = E/\rho - u^2/2 \tag{17}$$

$$V = 1/\rho \tag{18}$$

and the Grüneisen parameter is defined as

$$\Gamma = V\left(\frac{\partial p}{\partial e}\right)_V = \frac{\Gamma_0\rho_0}{\rho} \tag{19}$$

where ρ_0 is the density of the unstressed material.

The expression for $f(V)$ in Eq. (16), to accommodate for negative pressure (tension) and preserve positive sound speed squared, is

$$f(V) = \begin{cases} \dfrac{\rho_0 c_0^2\varphi}{(1-s\varphi)^2}\left[1 - \dfrac{\Gamma}{2V}(V_0 - V)\right] & \text{if} \quad V \le V_0 \\ c_0^2\left(\dfrac{1}{V} - \dfrac{1}{V_0}\right) & \text{if} \quad V > V_0 \end{cases} \tag{20}$$

where $\varphi = 1 - V/V_0$. The choice in Eq. (20) is required because for low energy and low pressure (as in a rarefaction) roundoff and approximation errors can result in negative values of c_0^2 because f' changes sign. To correct this, and following the approach of Miller and Puckett[22] and Arienti et al.,[23] the e.o.s. is extended with a pseudo-elastic-solid e.o.s.

The sound speed is given by

$$c_0^2 = \left(\frac{\partial p}{\partial \rho}\right)_e + \frac{p}{\rho^2}\left(\frac{\partial p}{\partial e}\right)_\rho = \Gamma e + f'(V) + \Gamma\frac{p}{\rho} \tag{21}$$

B. Governing Equations for Axisymmetric Deformation

With the preceding constitutive laws to describe material behavior, the equations governing axisymmetric deformation and flow of the material can be written in an Eulerian framework (with x denoting the radial coordinate and y the axial coordinate) as a system of conservation laws using the primitive variables as

$$\frac{\partial Q}{\partial t} + \frac{\partial F(Q)}{\partial x} + \frac{\partial G(Q)}{\partial y} = S(Q) \tag{22}$$

where the vector of conserved variables ($\boldsymbol{Q}$) and the convective flux vectors $\boldsymbol{F}(Q)$ and $\boldsymbol{G}(Q)$ are

$$\boldsymbol{Q} = \begin{Bmatrix} \rho \\ \rho u \\ \rho v \\ E \\ \rho s_{xx} \\ \rho s_{yy} \\ \rho s_{xy} \end{Bmatrix} \quad \boldsymbol{F}(Q) = \begin{Bmatrix} \rho u \\ \rho u^2 + p \\ \rho uv \\ u[E+p] \\ \rho u s_{xx} \\ \rho u s_{yy} \\ \rho u s_{xy} \end{Bmatrix} \quad \boldsymbol{G}(Q) = \begin{Bmatrix} \rho v \\ \rho uv \\ \rho v^2 + p \\ v[E+p] \\ \rho v s_{xx} \\ \rho v s_{yy} \\ \rho v s_{xy} \end{Bmatrix} \tag{23}$$

The preceding equations, written in conservative form, include the evolution of the deviatoric stresses. The dilatational part of the stress is obtained from an equation of state as given in Eq. (16). The source vector that appears in Eq. (22) is of the form:

$$S(Q) = \begin{Bmatrix} -\dfrac{\rho u}{x} \\ \dfrac{\partial s_{xx}}{\partial x} + \dfrac{\partial s_{xy}}{\partial y} + \dfrac{s_{xx} + s_{yy} + s_{xy}}{x} - \dfrac{\rho u^2}{x} \\ \dfrac{\partial s_{xy}}{\partial x} + \dfrac{\partial s_{yy}}{\partial y} + \dfrac{s_{xy}}{x} - \dfrac{\rho uv}{x} \\ S_E \\ S_{s_{xx}} \\ S_{s_{yy}} \\ S_{s_{xy}} \end{Bmatrix}$$

where

$$S_E = -\left[\frac{u(E+p)}{x} + \frac{(us_{xx} + vs_{yy})}{x}\right] + \frac{\partial}{\partial x}(us_{xx} + vs_{yy}) + \frac{\partial}{\partial y}(us_{xy} + vs_{yy}) \tag{24a}$$

For the deviatoric stress equations, the source terms are as follows:

$$S_{s_{xx}} = s_{xx}\left(\frac{\partial u}{\partial x} + \frac{\partial v}{\partial y}\right) + 2\Omega_{xy}s_{xy} + 2G\left[\frac{\partial u}{\partial x} - \Sigma\right] \tag{24b}$$

$$S_{s_{yy}} = s_{yy}\left(\frac{\partial u}{\partial x} + \frac{\partial v}{\partial y}\right) + 2\Omega_{yx}s_{xy} + 2G\left[\frac{\partial v}{\partial y} - \Sigma\right] \tag{24c}$$

$$S_{s_{xy}} = s_{xy}\left(\frac{\partial u}{\partial x} + \frac{\partial v}{\partial y}\right) + \Omega_{xx}s_{xy} + \Omega_{xy}s_{yy} - \Omega_{xy}s_{xx} - \Omega_{yy}s_{xy} + 2G\left[\frac{1}{2}\left(\frac{\partial u}{\partial y} + \frac{\partial v}{\partial x}\right)\right] \tag{24d}$$

where

$$\Sigma = \frac{1}{3}\left(\frac{\partial u}{\partial x} + \frac{u}{x} + \frac{\partial v}{\partial y}\right)$$

The equation for evolution of the plastic strain in Eulerian frame is

$$\frac{\partial \bar{\varepsilon}^p}{\partial t} + \boldsymbol{U} \cdot \nabla \bar{\varepsilon}_p = \sqrt{\frac{2}{3} tr\left(D_{ij}^p D_{ij}^p\right)} \tag{25}$$

where U is the velocity vector. The eigenvalues of the equation system (23), without the source terms included, were found to be real for the range of parameters, that is, material properties and impact velocities of interest in this work. Analysis of the conditions under which the system is expected to be hyperbolic has been performed in earlier work by the present authors. For a one-dimensional formulation, the eigenvalues are[20]

$$\lambda_1 = \lambda_2 = \lambda_3 = u \tag{26a}$$

$$\lambda_4 = c_0 + u \tag{26b}$$

$$\lambda_5 = c_0 - u \tag{26c}$$

The sound speed depends on the particular equation of state chosen for the pressure and is given next for the case of the Mie–Grüneisen equation of state. Note that for the set of calculations performed in this paper, the system is inertia dominated, and a Courant–Friedrichs–Lewy (CFL) criterion was used to obtain stable calculations. In the calculations shown, this criterion sufficed, and treating the source terms explicitly did not occasion numerical difficulties. However, an investigation of the overall system to ascertain hyperbolicity for a wider range of parameter space will be necessary to extend the present method.

The present system of equations is first solved using the essentially-nonoscillatory (ENO) numerical scheme[24,25] as will be described in a subsequent section. The radial return algorithm is then applied to bring the stress state back to the yield surface if the stress state falls outside of it. Equation (25) for the effective plastic strain is solved separately using a simple second-order upwind scheme.

IV. Numerical Method

The system of hyperbolic conservation laws given in Eq. (22) needs to be solved in a stable and accurate manner in the presence of moving boundaries embedded on the fixed Cartesian mesh. To capture the nonlinear wave propagation phenomena that arise in the high-speed impact situations of interest, a shock-capturing scheme is required. We apply a second order in space ENO scheme and a third-order TVD Runge–Kutta time stepping to solve the preceding system of equations. Detailed description of the numerical method, interface tracking, treatment of boundary conditions, contact algorithm, and validation is given in previous papers.[19,20] The method has been extensively validated for problems involving high strain-rate deformation in the presence of severely deforming interfaces between multiple materials.

A schematic of a typical case studied is shown in Fig. 1. The axisymmetric void is placed in the center of the computation domain, and various loading conditions are applied on the lower surface of the domain, that is, in the solid material. A condensed-phase, HMX (cyclo-tetramethylene-tetranitramine, $C_4H_8N_8O_8$) energetic material is considered in this study. HMX is a commonly used energetic crystal in heterogeneous propellants and explosives, and its physical properties are fairly well characterized.[9,15,26] The thermal diffusivity, $\kappa = 4 \times 10^{-10}$ kJ/m $\cdot$ μs $\cdot$ K, viscosity, $\eta = 310$ *Poise* for temperature below melting, 0.14 *Poise* above melting, specific heat, $C_V = 1000$ J/kg $\cdot$ K, material yield strength, $Y = 0.26$ GPa below melting, 0 above melting, room temperature, $T_0 = 300$ K.

Conley[27] has shown that the effect of compression on the melting point of the energetic material is very important in order to correctly represent the dynamics of void collapse. The phase transitions in the shocked material result in a softening of the material, and when the solid finally transitions to liquid phase the material loses strength, and therefore the yield stress is set to zero in the liquid phase. The melting temperature of the shocked explosive is modeled as a function of volume change. This relationship is estimated based on the Kraut–Kennedy[28] relation as follows:

$$T_m = T_{m0}[1 + a(\Delta V / V_0)] \tag{27}$$

where $a = 2(\Gamma - \frac{1}{3})$ and T_{m0} is the melting temperature at ambient condition, V_0 is the initial specific volume, and ΔV is the change in specific volume.

Table 1 HMX material properties[15,27]

Parameter	Value
ρ, kg/m^3	1900
C, J/kg-K	1000
T_m, K	520
s	2.38
Y, GPa	0.26
G, GPa	10.0
Γ	1.1
C_0, m/s	2650
κ, W/m-K	0.4
M, Poise	$310\ T < T_m$ $0.14\ T \geq T_m$

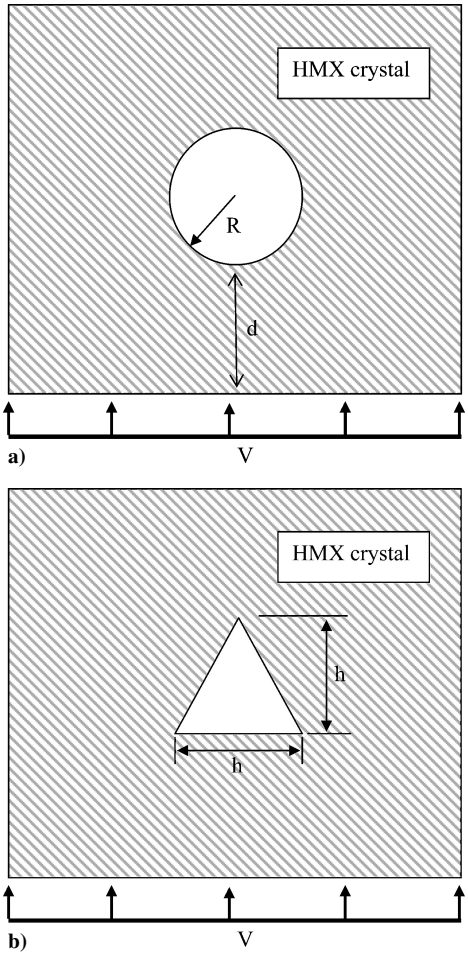

Fig. 1 Illustrations of the computational setup: a) idealized spherical void and b) idealized triangular void.

The parameters for the equation of state for the material as well as other material properties are given in Table 1.

Characteristic timescales (void collapse and shock passage) are estimated as follows. The shock velocity u_s is calculated, and the characteristic shock passage time for a void of radius r is

$$t_p = 2r/u_s \tag{28}$$

The characteristic time of void collapse is calculated as the difference between the total time taken for the complete collapse of the void and the time for the shock to travel a distance d before contacting the void. Referring to Fig. 1,

$$t_\mu = t_t - d/u_s \tag{29}$$

where t_t is the total collapse time.

V. Results

A. Inert Void Collapse in an HMX Crystal

The methodology developed in Udaykumar et al.[19] and Tran and Udaykumar[20] is applied in this chapter to study the collapse of a void is a material that is subjected to shock loading. Here the focus is on identifying the important mechanisms in the collapse of a void without consideration of chemical reactions in the solid and gas phases. We also confine attention to the solid-phase deformation behavior and the rise in temperature of the solid phase caused by shock-induced compression and plastic deformation. The physics of collapse of voids in the absence of chemical reactions is only partially relevant to energetic materials. However, deferring chemistry to that discussed in Tran and Udaykumar[21] allows for isolation of purely mechanical effects during void collapse and its result, which is the creation of high-temperature localized zones or hot spots.

B. Grid-Independence Study

To establish the framework for further calculations, grid independence of solutions is assessed for a typical test case for a void of 10 μm diam. The loading velocity is 500 m/s. This is the particle velocity that is supplied to the lower boundary of the computational domain, causing a compression wave to propagate upward to the void. Four mesh sizes are considered: 50×100, 100×200, 150×300, and 200×400. The effect of grid size on the temperature field produced by the void collapse is shown in Fig. 2. As seen in the figures, the maximum temperatures achieved are higher for the finer meshes. For the under-resolved mesh (50×100), the maximum temperature reached as well as the time when the significant rise in temperature occurs is inaccurate. For higher mesh resolution, the maximum temperatures as well as the time are comparable. For the 150×300 mesh, a grid-independent solution can be considered to have been reached. Similar conclusions can be arrived at from the plots of the ratio between total internal energy [$\int (\rho e)\, \mathrm{d}V$ integrated over the whole domain] and total kinetic energy [$\int (\frac{1}{2}\rho v^2)\, \mathrm{d}V$ integrated over the computational domain] vs time (Fig. 3). Notice that the instant (in time) where the major changes in regimes (changes in the slopes) occur are comparable for the 150×300 and 200×400 meshes. All calculations presented next are therefore carried out using a 150×300 mesh.

C. Spherical Void Collapse in an Elastoviscoplastic HMX Material

A spherical void with a radius of 5 μ, within a HMX material, undergoes axisymmetric deformation as a result of a propagating shock created by imposing a particle velocity at the bottom boundary. A schematic of the problem is shown in Fig. 1a. To remove the

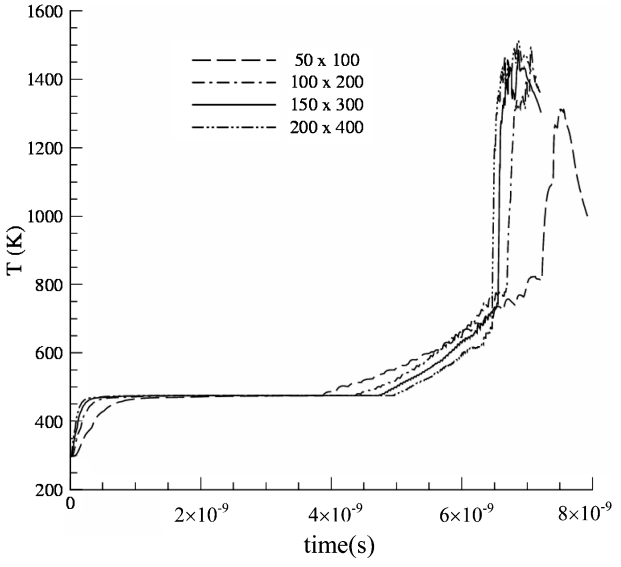

Fig. 2 Elastoviscoplastic, grid-refinement study with initial loading velocity of 500 m/s and initial void radius of 5 μm. Plot of maximum temperature vs time.

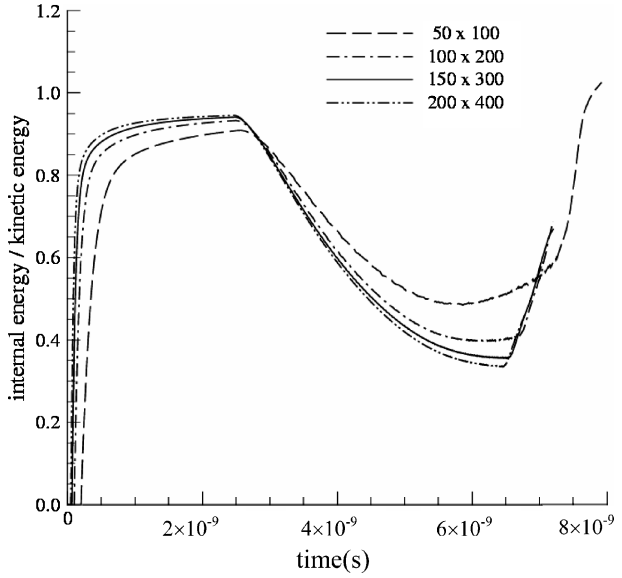

Fig. 3 Elastoviscoplastic, grid-refinement study with initial loading velocity of 500 m/s and initial void radius of 5 μm. Plot of the ratio between total internal energy and total kinetic energy vs time.

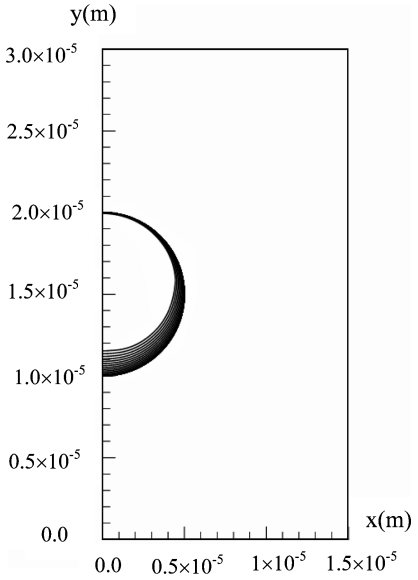

Fig. 4 Evolution of void collapse process for elastoviscoplastic, initial loading velocity of 50 m/s, 5-μm radius.

rise time from the already fairly extensive list of control parameters, the shock profile in the following cases is assumed to have zero rise time. The impulsive velocity supplied at the bottom boundary seeks to simulate the effect of impact at the bottom surface of the energetic material (Fig. 1). The material response is modeled using an elastoviscoplastic model, with constants shown in Table 1. The wave moves through the solid and is transmitted out through the upper boundary. The right boundary is subjected to symmetry conditions, whereas the left boundary is the axis of symmetry. The simulation is carried out for three different initial velocities: 50, 500, and 2000 m/s, using a 150 × 300 mesh. Void collapse can occur in different modes depending on the strength of the impinging shock. As the shock strength increases, the void collapse goes from a nearly spherical viscoplastic mode to a hydrodynamic mode where the lower surface of the void forms a jet, which impacts on the upper surface at high velocity. This transition is studied in the following computations.

Figure 4 shows the evolution of the void shape as this weak shock passes over it. The deformation of the void is weak in this case be-

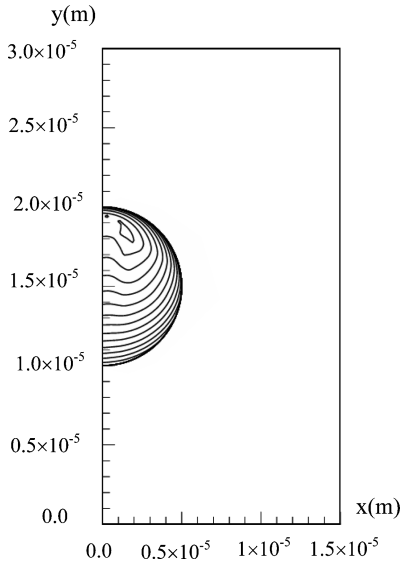

Fig. 5 Evolution of void collapse process for elastoviscoplastic, initial loading velocity of 500 m/s, 5-μm radius.

cause the resulting pressure rise from the shock wave passage is lower than the yield strength of the material. The temperature rises by only a few degrees as a result of the passing shock wave and deformation of the lower surface of the void. Figure 5 shows the void collapse evolution, jetting of the void lower surface, and the eventual complete collapse of the void for a higher loading condition, corresponding to an impact velocity of 500 m/s. In this case the energy of the shock wave itself causes a temperature rise of 30 K in the material (Fig. 6b). As the lower void surface caves in under the strength of the oncoming shock, a jetting phenomenon is observed. The lower surface of the void is traveling at high velocity in this case leading to the formation of a protrusion or jet. The plastic work done in deforming the void yields local temperature increases of over 250 K even before the jet impacts the top surface (Fig. 6f). Because of the large jetting velocity of the lower surface, the impact of the fast-moving lower surface with upper surface (Figs. 6c–6f) of the void causes a spherical shock wave that forms at the impact location and travels outward. The maximum temperature is over 1000 K, much higher than the rise caused by plastic work done on the void.

At still higher loading velocity of 2000 m/s, a true hydrodynamic mode can be discerned. While the lower surface forms a high-velocity jet, the upper surface does not move in this case as shown in the void shape evolution in Fig. 7. Upon collapse of the void, a secondary shock wave that is even stronger than the initial impact shock emanates from the point of collapse. This secondary shock is seen to interact with and intensify the initial shock wave (Figs. 8e–8h). This reinforcement of the impinging shock wave by pure mechanical collapse of a void can have important consequences on the loads imposed on a void that is downstream of the void in question. Once the shock interacts with the lower void surface, plastic deformation occurs quickly, which raises the temperature to around 1200 K even before the hydrodynamic impact (see Fig. 9). The final maximum temperature rises to about 2700 K (Fig. 9).

The contribution of the rise in temperature as a result of the different modes of energy deposition can be gathered from Fig. 9a. This plot shows the maximum temperature achieved for different loading strengths for a fixed void radius of 5 μm. For very low shock strength (the 50-m/s case), the temperature rise is limited to a few degrees Kelvin. For moderate shock strength (the 500-m/s case), the temperature rise in the bulk caused by shock passage alone is 150 K, plastic deformation at the void surface further increases the temperature by 250 K, and hydrodynamic impact caused by void collapse leads to a spike in temperature of about 700 K. For the highest shock strength studied (the 2000-m/s case), shock passage alone gives rise to about 800 K temperature rise in the bulk of the material, plastic

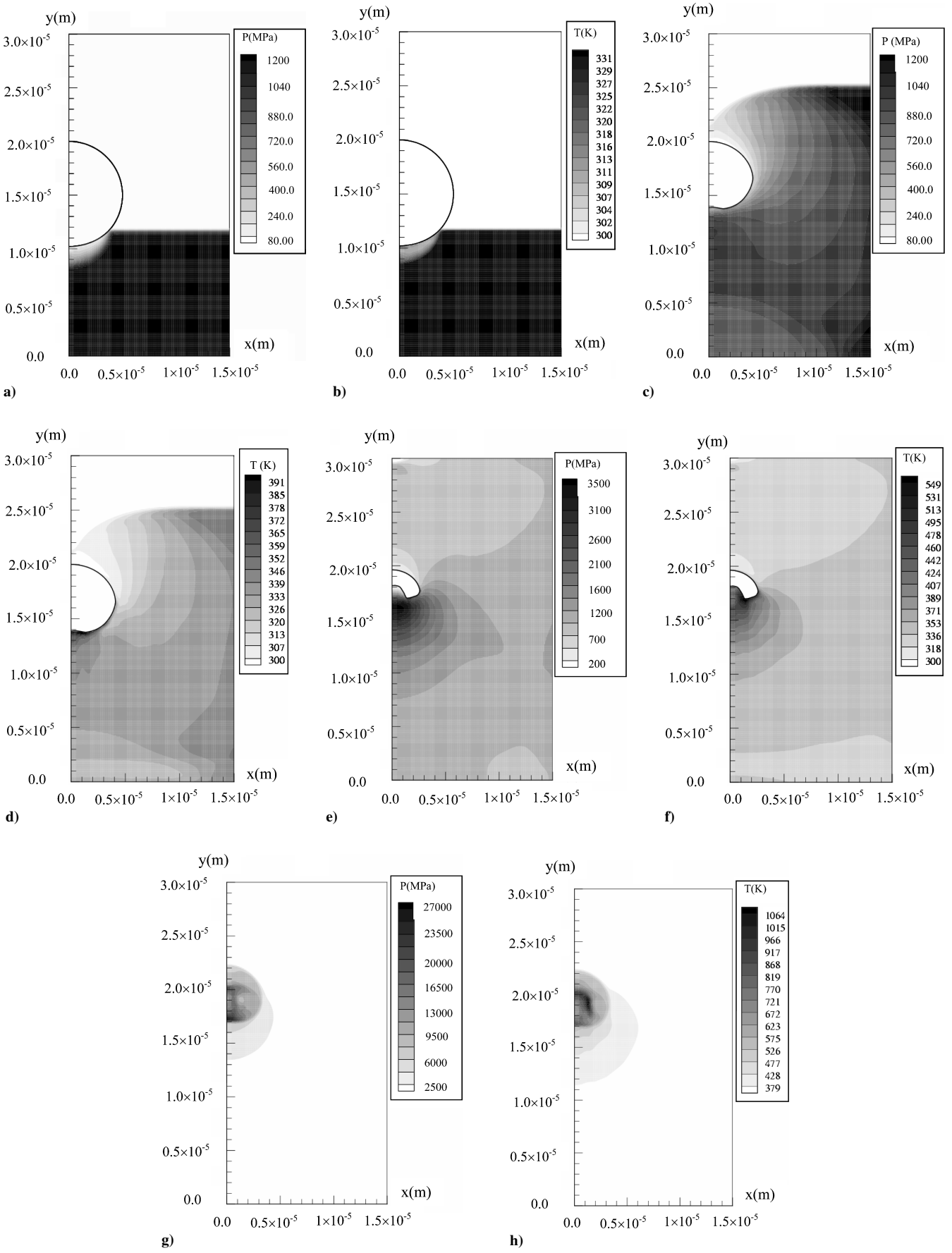

Fig. 6 Elastoviscoplastic, initial loading velocity of 500 m/s, 5-μm radius: a) pressure at 3.5 ns, b) temperature at 3.5 ns, c) pressure at 7.5 ns, d) temperature at 7.5 ns, e) pressure at 9.5 ns, f) temperature at 9.5 ns, g) pressure at 10.4 ns, and h) temperature at 10.4 ns.

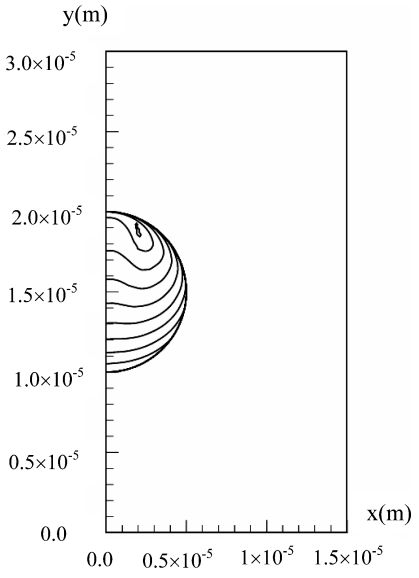

Fig. 7 Evolution of void collapse process for elastoviscoplastic, initial loading velocity of 2000 m/s, 5-μm radius.

deformation of the void surface leads to a rise of 100 K in the temperature, and hydrodynamic impact at void collapse contributes to a 1500 K rise in the temperature at the collapse site. In general, for lower initial applied loadings the temperature rise caused by plastic work is more significant. As the loading increases, the void collapse time is shortened, and plastic work loses its dominance to the hydrodynamic jet impact mode of energy localization. Thus, for the highest loading considered (i.e., for the 200-m/s case) the temperature rise to plastic work is a small fraction of the rise caused by hydrodynamic impact.

Another perspective can be gained by considering the variation of the energy deposition process (Fig. 9b). To investigate the effectiveness of conversion of energy as a result of void collapse, the ratio of the total internal energy $[\int (\rho e)\,\mathrm{d}V$ integrated over the whole domain] to the kinetic energy $[\int (\frac{1}{2}\rho v^2)\,\mathrm{d}V$ integrated over the computational domain] as a function of time for various impact velocities is plotted in Fig. 9b. For each of the computed impact velocities, the initial part of the curve with zero slope represents the rise in the energy state during the time taken by the shock to reach the void. Once the shock wave contacts the void lower surface, there is rise in kinetic energy caused by void deformation as indicated by the negative slope. In general, we see that there are three distinct stages which define the void collapse process. In the first, the conversion of the energy of the shock to kinetic energy caused by acceleration of material on the lower surface of the void occurs (the negative slope region). However once the material starts to accelerate plastic deformation ensues, and the material begins to resist the deformation (the low positive slope region). The plastic work then dissipates as heat and raises the internal energy of the material. In the final stage the lower void surface impacts on the upper surface, and the void closes, leading to conversion of the excess kinetic energy of the lower surface into thermal energy (the abrupt rise region). With increasing impact velocities there is a gradual transition in the relative significance of the three distinct phases in the energy deposition process. For a loading velocity of 50 m/s, for which the shock strength marginally exceeds the material yield strength, only the first two stages in the void collapse process exist. In this case the kinetic energy first rises above the internal energy because the lower surface of the void accelerates and the void deforms. However, the plastic deformation results in increase of the thermal energy because of work done in deforming the material. The void does not completely collapse, and therefore the final stage of impact does not exist. For the 200-m/s loading conditions, one can begin to see the three different stages, namely, acceleration, plastic work raising the internal energy, and hydrodynamic impact. The jetting regime is clearly the most effective way to raise the internal energy of the void-collapse process. For higher loading condition, for example 2000 m/s, the second stage, namely, the plastic work becomes insignificant in the energy deposition process. Only two regimes are evident, namely, the increase in kinetic energy caused by the deformation of the void and resulting jet formation and the hot spot caused by jet impact. In fact, for this high-velocity case, because the plastic work does not appear to contribute to the energy localization at all, this case can be considered to be purely "hydrodynamic."

The effect of the void radius on temperature rise is shown in Fig. 10a for a loading velocity of 500 m/s. For void radius below 2 μ the temperature rises steeply with increasing radius of the void. This temperature rise is predominantly caused by the viscoplastic work done in deforming the void. The maximum temperature rise as a result of viscoplastic deformation occurs for a void of around 2.0-μm radius. For larger sized voids the contribution of the viscoplastic work to the temperature rise decreases. On the other hand, the temperature rise as a result of hydrodynamic impact increases for void radii larger than 2 μ. The net effect is that there is overall a weak rise in the temperature at the hot spot for the larger radius voids. The oscillations in temperature observed at the end of the collapse process for the larger void sizes are caused by squeezing and collapse of the smaller voids that are formed after the impact of the jet formed by the lower void surface. This figure indicates there exists a critical void radius where the temperature rise from hydrodynamic impact (because of the jetting velocity) becomes only weakly dependent on void radius. It also clearly indicates that there is a direct correlation between the jet formation (and its kinetic energy) and the local temperature rises that can lead to hot-spot formation. For smaller voids the collapse time is low, and the jet velocity is unable to reach high values before the entire void collapses. For voids that are large enough (this being a function of the impact velocity), the collapse time is long enough for the lower surface to be accelerated to a state where the material strength is inconsequential and the jet velocity saturates.

Figure 10b shows the energy deposition behavior as a function of time for various void radii with loading velocity of 500 m/s. For smaller void radii (0.5 and 1.0 μm), the initial shock passes through without much energy being extracted for plastic deformation of the void. For void radius of up to 5 μm, two regimes are observed, the acceleration (increase in kinetic energy) and the hydrodynamic impact stages. For this intermediate-sized void the collapse time is too low for the plastic work to play a major role in the energy localization process. For higher void radii, a small region where viscoplastic work also contributes to the heating of the void is observed. However, the predominant mode leading to internal energy rise is the hydrodynamic impact of the lower void surface on the upper void surface.

D. Triangular Void Collapse Results in an Elastoviscoplastic MHX Material

To assess the effect of void shape on the hot-spot energies, we study triangular voids and compare their behavior with spherical voids. Two different orientations of a triangular void (Fig. 1b) are considered, one with the apex pointing away from the incoming shock (TUP) and the other with the apex pointing toward the incoming shock (TDOWN), both with initial loading velocity of 500 m/s. For the TUP case shown in Figs. 11a, it is observed that there is no jetting along the axis of symmetry. However, there is jetting and void closure that occurs around the bottom corner of the triangle. Although the jetting is small because jetting velocities do not have the time to build up, the rise in temperature is significant. This closure of the bottom corner occurs repeatedly as the void collapses as shown in the evolution of the void shape in Fig. 11a. These small collapsing pores could probably play an important part in the rise in internal energy. It is not possible to fully resolve such events within the present mesh limitations however, and no firm quantitative conclusions can be made regarding their role.

The case with apex pointing toward the incoming shock (TDOWN) is shown in Fig. 11b. At the time of 5.5 ns (see Figs. 12a), the temperature rise in this case is only around 400 K because of plastic work alone, whereas for the TUP case the value is around

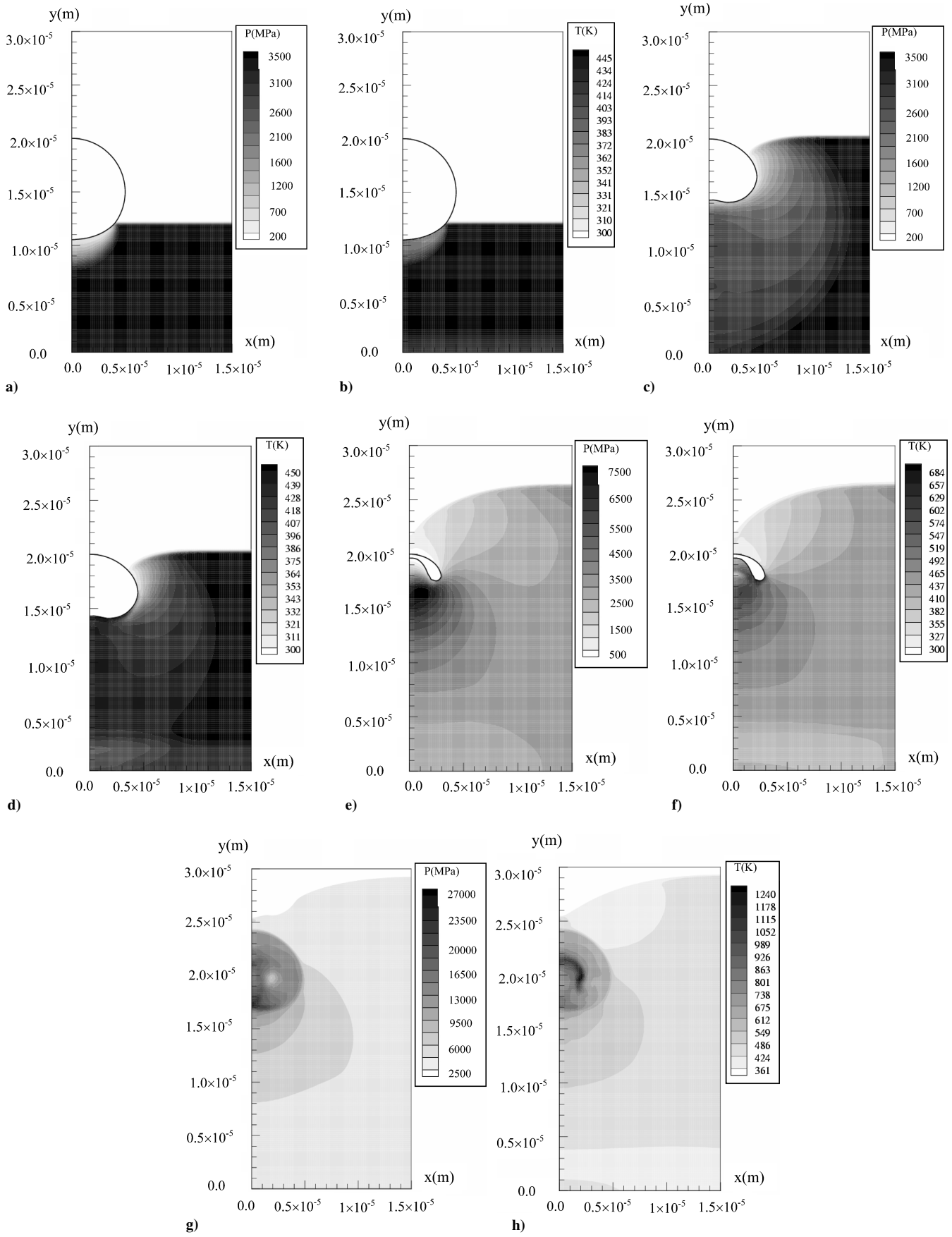

Fig. 8 Elastoviscoplastic, initial loading velocity of 2000 m/s, 5 μm radius: a) pressure at 3.0 ns, b) temperature at 3.0 ns, c) pressure at 5.0 ns, and d) temperature at 5.0 ns.

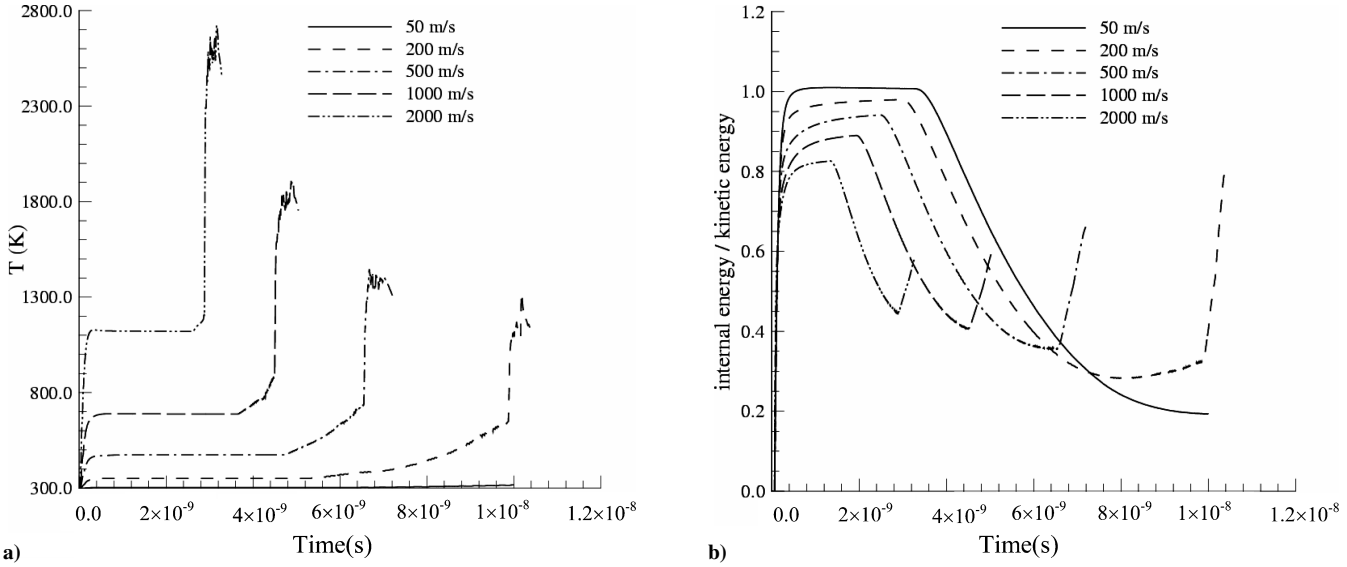

Fig. 9 Void collapse behavior for various loading conditions, elastoviscoplastic case, 5-μm radius void: a) maximum temperature vs time and b) ratio of total internal energy to total kinetic energy vs time.

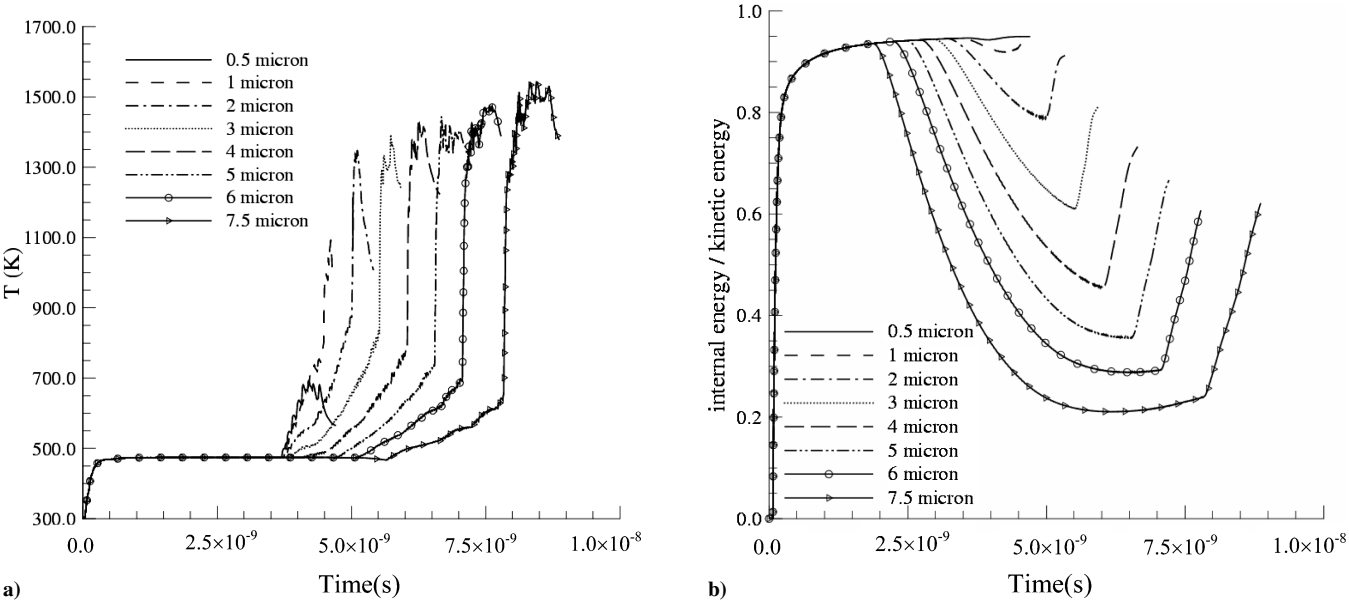

Fig. 10 Void collapse behavior for various loading conditions, elastoviscoplastic case, 5-μm radius void, 500 m/s loading velocity: a) maximum temperature in the domain vs time and b) ratio of total internal energy to total kinetic energy vs time.

800 K. The much larger temperature rise of the TUP configuration compared to that of TDOWN is caused by small jetting and impact that occurs almost continuously in the void-collapse process around the corner of the triangle. As the TDOWN void continues to deform, jetting is clearly observed along the axis of symmetry (Fig. 11b), eventually impacting the upper void surface. At the completion of the void-collapse process, the maximum temperature rise is around 1500 K, compared with the TUP case where it is 2600 K.

The orientation of the void with respect to the incoming shock clearly has an impact on the intensity of hot-spot formation. Intuitively, one would think that the TDOWN case would be more efficient in focusing shock energy into a hot spot because of the presence of the low-strength sharp edge facing the oncoming shock, but the calculated results show otherwise. A series of small jets and pinching of the corner appears to be more effective in raising the thermal energy than a larger single jet.

Figure 12b compares the effectiveness of energy conversion for the three different voids: spherical, TUP, and TDOWN, for an initial loading velocity of 500 m/s. For the spherical void, one can distinguish three different energy regimes, although the regime in which plastic work is converted to internal energy is cut short by the hydrodynamic impact regime. For the TDOWN case, the regime in which kinetic energy dominates is clear and lasts over much of the collapsing time. Towards the end, a weak hydrodynamic impact is shown by a modest (compared to spherical void case) rise in the internal energy. For the TUP case, although there appears to be a continuous series of small jets impacting the upper void surface, the rise in internal energy is still small compared to that in the kinetic energy during the initial phase of the collapse. The second regime in which conversion of plastic work to heat is significant is shown in the positive slope part of the curve for that case. Towards the end of the collapse process, there is no clear hydrodynamic regime. However, the conversion to internal energy is more effective compared to the other two geometries caused by the series of small jets that impact at the corner of the collapsing void. Thus, the precise balance of energy contributions in the collapse of a void in an inert material depends quite significantly on the shape of the collapsing void and its orientation with respect to the impinging shock.

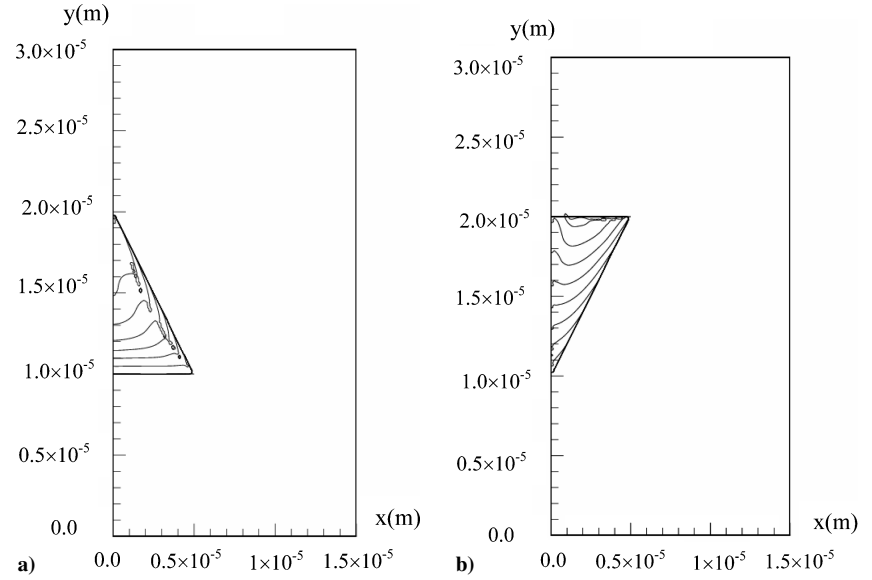

Fig. 11 Evolution of void collapse in the elastoviscoplastic case, initial loading velocity of 500 m/s: a) triangular void up and b) triangular void down.

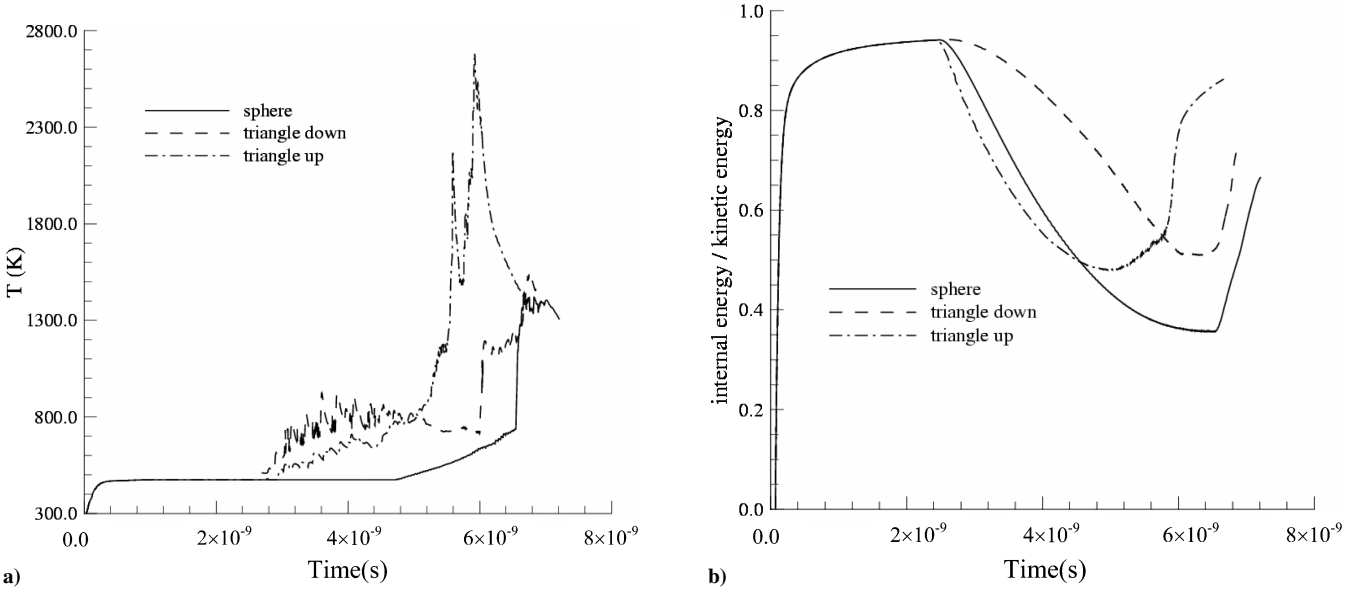

Fig. 12 Results of void collapse in the elastoviscoplastic case, loading velocity of 500 m/s: a) maximum temperature vs time for three different void shapes and b) ratio of total internal energy to total kinetic energy vs time for the different shapes.

VI. Conclusions

A numerical technique developed for the simulation of high-strain-rate, large deformation calculations involving multimaterial interactions was applied to study the collapse of voids in a material with the mechanical properties corresponding to HMX. The effect of imposing a shock loading on an axisymmetric void was studied to investigate whether there are clearly discernible regimes where the collapse of a void and the accompanying energy localization are caused by viscous and hydrodynamic effects. Based on these calculations the following conclusions were drawn:

The temperature rise caused by plastic work in deforming the void is larger compared to the rise as a result of the dissipation of kinetic energy of the passing shock wave. The largest temperature rise is caused by the hydrodynamic impact of the jet. The void collapse and hot-spot formation events (at any impact velocity) in every case consist of a mixture of viscoplastic and hydrodynamic effects. No clear Reynolds-number regimes were found as postulated by one-dimensional spherically symmetric analyses conducted by Khasainov and other authors.

There are three distinct phases in the void-collapse process: acceleration of the lower void surface (an increase in kinetic energy), an increase in internal energy caused by plastic work, and hydrodynamic impact. The hydrodynamic jetting regime is the most effective way to raise the internal energy.

The rise in temperature approaches an asymptotic value for void radius higher than 2.0–3.0 μm. This indicates there indeed exists a critical void radius beyond which the effect of size on the void collapse process becomes weak. However below this critical radius void size does have a strong effect on energy localization. Void shape and its orientation with respect to the incoming shock have an impact on the intensity of hot-spot formation. For triangular voids, a series of small jets and pinching of the corner appears to be more effective in raising the thermal energy than a larger single jet.

In Tran and Udaykumar[21] we consider the effects of the gas phase on the mechanics of void collapse. The chemical reactions that occur in the condensed and gas phases are also included in the model to simulate the collapse of the void, energy localization, and the effects of these on the reaction initiation at the void location.

Acknowledgments

The work presented here was supported by grants to H. S. Udaykumar from the Computational Mechanics Branch at Air Force Research Laboratory–MNAC, Eglin, Florida (Project Manager: Joel Stewart) and the Air Force Office of Scientific Research Computational Mathematics program (Project Manager: Fariba Fahroo).

References

[1]Bowden, F. P., and Yoffe, A. D., *Initiation and Growth of Explosions in Liquids and Solids*, Cambridge Univ. Press, New York, 1951, p. 102.

[2]Khasainov, B. A., Borisov, A. A., Ermolaev, B. S., and Korotkov, A. I., "Two Phase Visco-Plastic Model of Shock Initiation of Detonation in High Density Pressed Explosives," *Proceedings—Seventh Symposium (International) on Detonation*, White Oak, MD, 1982, pp. 435–447.

[3]Mader, C., "Initiation of Detonation by the Interaction of Shock with Density Discontinuity," *Physics of Fluids*, Vol. 8, No. 10, 1965, pp. 1811–1816.

[4]Starkenberg, J., "Ignition of Solid High Explosive by the Rapid Compression of an Adjacent Gas Layer," *Proceedings—Seventh Symposium (International) on Detonation*, White Oak, MD, 1982, pp. 3–16.

[5]Kang, J., Butler, P. B., and Baer, M. R., "Thermomechanical Analysis of Hot Spot Formation in Condensed-Phase, Energetic Materials," *Combustion and Flame*, Vol. 89, No. 2, 1992, pp. 117–139.

[6]Frey, R., "Initiation of Explosives by Rapid Shear," *Proceedings—Seventh Symposium (International) on Detonation*, White Oak, MD, 1981, pp. 36–42.

[7]Frey, R. B., "Cavity Collapse in Energetic Materials," *Proceedings—Eighth Symposium (International) on Detonation*, Office of Naval Research, Silver Spring, MD, 1985, pp. 385–393.

[8]Lee, E. L., and Tarver, C. M., "Phenomenological Model of Shock Initiation in Heterogeneous Explosives," *Physics of Fluids*, Vol. 23, No. 12, 1980, pp. 2362–2372.

[9]Menikoff, R., and Kober, E., "Compaction Waves in Granular HMX," Los Alamos National Lab., Rept. LA-13456-MS, Los Alamos, NM, 1999.

[10]Powers, J. M., "Two-Phase Viscous Modeling of Compaction of Granular Materials," *Physics of Fluids*, Vol. 16, No. 8, 2004, pp. 2975–2990.

[11]Gonthier, K. A., "Modeling and Analysis of Reactive Compaction for Granular Energetic Solids," *Combustion Science and Technology*, Vol. 175, No. 9, 2003, pp. 1679–1709.

[12]Gonthier, K. A., and Jogi, V., "Multiscale Shock Heating Analysis of a Granular Explosive," *Journal of Applied Mechanics*, Vol. 72, No. 4, 2005, pp. 538–552.

[13]Carroll, M. M., and Holt, A. C., "Static and Dynamic Pore-Collapse Relations for Ductile Porous Materials," *Journal of Applied Physics*, Vol. 43, No. 4, 1972, pp. 1626–1636.

[14]Powers, J. M., "Thermal Explosion Theory for Shear Localizing Energetic Solids," *Combustion Theory and Modeling*, Vol. 3, No. 1, 1999, pp. 103–122.

[15]Menikoff, R., and Sewell, T. D., "Constituent Properties of HMX Needed for Meso-Scale Simulations," *Combustion Theory and Modeling*, Vol. 6, No. 1, Feb. 2002, pp. 103–125.

[16]Benson, D. J., and Conley, P., "Eulerian Finite-Element Simulations of Experimentally Acquired HMX Microstructures," *Modeling and Simulation in Materials Science and Engineering*, Vol. 7, No. 3, 1999, pp. 333–354.

[17]McGlaun, J. M., Thompson, S. L., Kmetyk, L., and Elrick, M. G., "A Brief Description of the Three-Dimensional Shock Wave Physics Code CTH," Sandia National Lab., SAND89-0607, Albuquerque, NM, July 1990.

[18]Baer, M. R., Kipp, M. E., and van Swol, F., "Micromechanical Modeling of Heterogeneous Energetic Materials," *Proceedings—Eleventh (Internationa)l Detonation Symposium*, 1998.

[19]Udaykumar, H. S., Tran, L., Belk, D. M., and Vanden, K. J., "An Eulerian Method for Computation of Multimaterial Impact with ENO-Shock Capturing and Sharp Interfaces," *Journal of Computational Physics*, Vol. 186, No. 1, 2003, pp. 136–177.

[20]Tran, L., and Udaykumar, H. S., "A Particle-Level-Set-Based Sharp Interface Cartesian Grid Method for Impact, Penetration, and Void Collapse," *Journal of Computational Physics*, Vol. 193, No. 2, 2004, pp. 469–510.

[21]Tran, L., and Udaykumar, H. S., "Simulation of Void Collapse in an Energetic Material Part 2: Reactive Case," *Journal of Propulsion and Power* (to be published).

[22]Miller, G. H., and Puckett, E. G., "A High-Order Godunov Method for Multiple Condensed Phases," *Journal of Computational Physics*, Vol. 128, No. 1, 1996, pp. 134–164.

[23]Arienti, M., Morano, E., and Shepherd, J., "Nonreactive Euler Flows with Mie-Grüneisen Equation of State for High Explosives," California Inst. of Technology, Technical Rept. FM99-8, 1999, Pasadena, CA, pp. 1–56.

[24]Shu, C.-W., and Osher, S., "Efficient Implementation of Essentially Non-Oscillatory Shock-Capturing Schemes," *Journal of Computational Physics*, Vol. 77, No. 2, 1988, pp. 439–471.

[25]Shu, C.-W., and Osher, S., "Efficient Implementation of Essentially Non-Oscillatory Shock-Capturing Schemes II," *Journal of Computational Physics*, Vol. 83, No. 1, 1989, pp. 32–78.

[26]Conley, P. A., and Benson, D. J., "An Estimate of Solid Viscosity in HMX," *Proceedings of the 11th Symposium (International) on Detonation*, Office of Naval Research, Silver Spring, MD, 1998, pp. 272–289.

[27]Conley, P. A., "Eulerian Hydrocode Analysis of Reactive Micromechanics in the Shock Initiation of Heterogeneous Energetic Material," Ph.D. Dissertation, Dept. of Mechanical Engineering, Univ. of California, San Diego, CA, 1999.

[28]Poirier, J.-P., *Introduction to the Physics of the Earth's Interior*, Cambridge Univ. Press, Cambridge, England, U.K., 1991.